Chinese Journal of Chemical Engineering 65 (2024) 19–28

Contents lists available at ScienceDirect

Chinese Journal of Chemical Engineering

journal homepage: www.elsevier.com/locate/CJChE

Full Length Article

Enhanced stability of nitrogen-doped carbon-supported palladium catalyst for oxidative carbonylation of phenol

Xiaojing Liu [1], Ruohan Zhao [1], Hao Zhao [1], Zhimiao Wang [1,2,*], Fang Li [1,2,*], Wei Xue [1,2,*], Yanji Wang [1,2,3]

[1] Hebei Provincial Key Laboratory of Green Chemical Technology and High Efficient Energy Saving, School of Chemical Engineering and Technology, Hebei University of Technology, Tianjin 300130, China
[2] Tianjin Key Laboratory of Chemical Process Safety, Tianjin 300130, China
[3] Hebei Industrial Technology Research Institute of Green Chemical Industry, Huanghua 061100, China

ARTICLE INFO

Article history:
Received 10 May 2023
Received in revised form 27 July 2023
Accepted 6 August 2023
Available online 20 August 2023

Keywords:
Supported Pd catalyst
N-doped carbon
Amphiphilic triblock copolymer
Pyridinic nitrogen
Stability

ABSTRACT

Enhancing the stability of supported noble metal catalysts emerges is a major challenge in both science and industry. Herein, a heterogeneous Pd catalyst (Pd/NCF) was prepared by supporting Pd ultrafine metal nanoparticles (NPs) on nitrogen-doped carbon; synthesized by using F127 as a stabilizer, as well as chitosan as a carbon and nitrogen source. The Pd/NCF catalyst was efficient and recyclable for oxidative carbonylation of phenol to diphenyl carbonate, exhibiting higher stability than Pd/NC prepared without F127 addition. The hydrogen bond between chitosan (CTS) and F127 was enhanced by F127, which anchored the N in the free amino group, increasing the N content of the carbon material and ensuring that the support could provide sufficient N sites for the deposition of Pd NPs. This process helped to improve metal dispersion. The increased metal-support interaction, which limits the leaching and coarsening of Pd NPs, improves the stability of the Pd/NCF catalyst. Furthermore, density functional theory calculations indicated that pyridine N stabilized the Pd^{2+} species, significantly inhibiting the loss of Pd^{2+} in Pd/NCF during the reaction process. This work provides a promising avenue towards enhancing the stability of nitrogen-doped carbon-supported metal catalysts.

1. Introduction

Ultrafine metal nanoparticles (NPs) have been widely used in heterogeneous catalysis due to their high activity [1–3]. However, the stability of noble metal NP catalysts is hampered by agglomeration and leaching of NPs, or valence-state changes of the active species [4,5]. A typical reaction is oxidative carbonylation of phenol (OCP) to synthesize diphenyl carbonate (DPC). DPC is an essential chemical intermediate in fine chemical industry [6]. OCP is a multi-step electron transfer reaction and usually catalyzed by Pd compounds along with various co-catalysts. As research has advanced, the catalytic efficiency for OCP has been improved to some extent, whereas the recoverable performance of the catalyst is unsatisfactory [7,8]. The catalyst often undergoes rapid deactivation after only one use, which is mainly because of reduction of Pd (II) active species as well as leaching and aggregation of Pd NPs [9–11]. Generally, it is desirable to improve the stability of Pd NPs by loading them on a heteroatom-doped support [12,13]. Therefore, design and synthesis of a functionalized support are essential to improve the stability of Pd-based catalysts in OCP.

Carbon-based materials possess the advantages of high surface area, controllable morphology and availability of chemical modifications, which have been widely employed in the heterogeneous catalysts as a support material [14]. Song *et al.* [15] indicated that activated carbon-supported Pd catalysts exhibited a higher DPC yield than the best homogeneous system for the same amount of Pd, owing to the better Pd dispersion on the activated carbon support. However, he discovered that the Pd-based catalyst tended to sinter in the enriched reducing CO atmosphere, resulting in inferior reusability. Atomic nitrogen, a typical heteroatom, has been introduced into the carbon framework by various methods as an anchor to improve the dispersion and stabilization of metal NPs [16]. Furthermore, the quantity of N-dopant and various N species are crucial for understanding the support effects on the coordination structure of the metal species, and thus the catalytic behavior

* Corresponding authors at: Hebei Provincial Key Laboratory of Green Chemical Technology and High Efficient Energy Saving, School of Chemical Engineering and Technology, Hebei University of Technology, Tianjin 300130, China.
E-mail addresses: wangzhimiao@hebut.edu.cn (Z. Wang), lifang@hebut.edu.cn (F. Li), weixue@hebut.edu.cn (W. Xue).

https://doi.org/10.1016/j.cjche.2023.08.001
1004-9541/

[5,17–20]. Mao *et al.* [21] remarked that graphitic N might facilitate nucleation and dispersion, rather than serve as an anchor; whereas pyridinic N serves as anchors and dispersants. Accordingly, nitrogen-rich doped carbon materials with well-defined functional groups are ideal supports for anchoring metal NPs. Chitosan (CTS), the second-most-abundant biomass after cellulose, consists of ~40% carbon and ~8% nitrogen [22,23]. Because of the —NH_2 and —OH as functional groups, CTS exhibits excellent chelating properties and electrostatic attraction to metals, and can be utilized for adsorption as well as stabilization of metallic ions. The amino groups are protonated such that CTS is converted into cationic alkaline polysaccharides that exhibit a positive charge in dilute acid. Therefore, there is hydrogen bonding as well as electrostatic interactions between CTS and amphiphilic triblock copolymers (*e.g.*, Pluronic F127) with strongly electronegative atoms; this fact plays an important role in preparing stable and ideal catalysts [24]. Moreover, F127 can be used as a template for preparing nitrogen-doped mesoporous carbon materials, enhancing the accessibility of the active site of Pd NPs [25,26]. However, so far, there is no literature report on preparing CTS-derived, nitrogen-doped carbon-supported Pd catalysts for OCP.

Herein, nitrogen-doped carbon (NCF) was prepared by using an amphiphilic triblock copolymer (Pluronic F127) as the stabilizer, as well as chitosan as a carbon and nitrogen source. Then the Pd/NCF catalyst was prepared by wet impregnation. A control experiment was carried out by not adding F127; defined as Pd/NC. The Pd/NCF was first used for catalytic OCP to DPC and exhibited excellent activity as well as stability. Compared with Pd/NC, Pd/NCF exhibited higher stability. After the second cycle, the DPC yield was 91.3% of the initial yield. The high stability of Pd/NCF was investigated by a series of characterizations and density functional theory (DFT) calculations.

2. Experimental

2.1. Catalyst preparation

Typically, N-doped carbon was produced by hydrothermal treatment and high-temperature pyrolysis with using F127 as stabilizer. An ethanol solution containing F127 (0.01 $g{\cdot}ml^{-1}$, 100 ml) was mixed with HCl solution (0.1 $mol{\cdot}L^{-1}$) containing chitosan (0.02 $g{\cdot}ml^{-1}$, 150 ml), and heated to 50 °C and stirred vigorously until a homogeneous viscous solution was obtained. Then, the viscous solution was transferred into a Teflon-lined stainless autoclave and reacted at 200 °C for 15 h. The precipitation was collected by centrifugation and washed three times with H_2O and ethanol, respectively, and dried at 80 °C under vacuum to get the prepolymer labeled as pre-NCF. The prepolymer pre-NC was prepared through the same procedure only without using F127. The pre-NCF or pre-NC were transferred into a crucible and calcined under a flow of nitrogen, and the products were denoted as NCF and NC, respectively. Calcination procedure: the temperature was raised to 410 °C at the rate of 2 $°C{\cdot}min^{-1}$ and maintained for 2 h, and then heated to 800 °C at the rate of 5 $°C{\cdot}min^{-1}$ for 3 h.

The Pd/NCF catalyst was prepared by the conventional wet impregnation method. An aqueous solution of Na_2PdCl_4 was prepared using a $PdCl_2$ to NaCl molar ratio of 1:2. A 700 mg quantity of the presynthesized NCF support was dispersed in 30 ml of ultrapure water with sonicating, after which the Na_2PdCl_4 solution was added and the mixture under continuous stirring for 12 h. The precipitation was collected by centrifugation and dried at 80 °C for 12 h. Finally, the precipitation was calcined at 150 °C for 4 h under N_2 flow, the product was denoted as Pd/NCF. Pd/NC was prepared using NC as support by the same method. The nominal Pd loading in the two catalysts was 1% (mass).

2.2. Catalyst characterization

X-ray diffraction (XRD) patterns were carried out through a Bruker D8 FOCUS X-ray diffractometer with Cu K_α radiation (λ = 0.15406 nm). Raman spectra were measured on a Renishaw inVia Raman Microscope. The N_2 adsorption–desorption isotherms were measured on a Micromeritics ASAP 2020 instrument. The specific surface area was calculated using the Brunauer–Emmett–Teller (BET) method. The pore size distribution was determined through the Barrett–Joyner–Halenda (BJH) model. The Fourier transform infrared (FTIR) spectra was conducted with the TENSOR 27 FT-IR spectrometer. The valence of the elements present in samples were studied *via* X-ray photoelectron spectroscopy (XPS) with Al K_α X-ray source. Transmission electron microscope (TEM) images and high angle annular dark field scanning (HAADF-STEM) images were recorded on a FEI Talos F200s microscope. The Pd content was measured by a Thermo ICAP PRO 7300 inductively coupled plasma (ICP)–optimal emission spectrometry (OES). The content of nitrogen element was determined using elemental analysis (Thermo Flash, EA 1112). The metal dispersion of catalysts was determined by CO pulse chemisorption, which was conducted on a fully automated chemisorption analyzer (Micromeritics, Autochem II 2920).

2.3. Catalytic activity evaluation

Typically, the Pd/NCF or Pd/NC catalyst, $Cu(OAc)_2$, tetrabutylammonium bromide (TBAB), hydroquinone (H_2BQ), desiccant (4A molecular sieve), phenol and CH_2Cl_2 were added into the stainless-steel autoclave of Amtech® Slurry Phase Reactor Systems, and sealed and purged with N_2 and filled with O_2 and CO [8]. The temperature was raised to 100 °C for 6 h reaction. After the reaction, the reactor was cooled and vented in a fume hood. Then the insoluble precipitates were removed by centrifugation, and the yield of DPC was measured by high performance liquid chromatography (HPLC).

A K2600 liquid chromatograph (Waters, America) was employed to conduct quantitative analysis of DPC and phenol, utilizing an external standard method. The chromatographic column was a Venusil XBP C18 (5 μm, 4.6 mm × 150 mm) with a flow rate of 0.6 $ml{\cdot}min^{-1}$ and a detection wavelength of 254 nm. The mobile phase was CH_3OH/H_2O (65/35, volume fraction) and the injection volume was 20 μl. The column temperature was set to 30 °C.

2.4. Recycling test

The reusability of the catalysts was evaluated. After the first reaction, the catalysts were collected by centrifugation and washed three times with ethanol. After heat treatment at 150 °C for 4 h, and reused in the next subsequent run.

2.5. Theoretical calculations

Theoretical models including pyridinic N (N-6), pyrrolic N (N-5), graphitic N (N-Q), oxidized N (N-O), Pd(II)-N-6, Pd(II)-N-5, Pd(II)-N-Q and Pd(II)-N-O were established for density functional theory (DFT) calculation. All the DFT calculations have been carried out by using the Vienna *ab initio* simulation package (VASP) [27]. The electron exchange correlation interaction employed the method of the generalized gradient approximation (GGA) with Perdew-Burke-Ernzerhof (PBE) functional [28]. The Brillouin zone integration was applied with a Monkhorst-Pack scheme with *k*-points grid of 2 × 2 × 1 and a 400 eV plane-wave energy cut-off. The convergence criteria were set to 1.0×10^{-5} eV for the energy and maximum force of 0.5 $eV{\cdot}nm^{-1}$, respectively. The adsorption energy of Pd(II) with different types of nitrogen-doped carbon

fragments was calculated as $E_{ads} = E(\text{model}) - E(\text{Pd}) - E(\text{fragment})$, where E(model), E(Pd) and E(fragment) are the energy of the model, the single Pd(II) and isolated initial different types of nitrogen-doped carbon fragments, respectively. All of the electron energies are adjusted using zero-point energy.

3. Results and Discussion

3.1. Activity of catalysts

The catalytic activity of Pd/NCF and Pd/NC catalysts for OCP was investigated, and the results were shown in Table 1. The phenol conversion of Pd/NCF was 45.9%, which was slightly less than that of Pd/NC (60.4%). The DPC selectivity of Pd/NCF was similar to that of Pd/NC.

The effect of F127 on the catalysts was then investigated by the characterization of Pd/NCF and Pd/NC. XRD patterns (Fig. 1(a)) indicate that Pd/NC exhibited two broad peaks centered at 22.9° and 43.0°, which are attributed to the (0 0 2) plane of disordered amorphous carbon and the (1 0 0) plane of graphite-like carbon, respectively [31]. After F127 was added, these two peaks in the Pd/NCF sample exhibited a slight positive shift to 23.8° and 43.8°, respectively, indicating that introducing F127 increased the graphitization of the obtained carbon material [32]. The diffraction peaks of Pd compounds were not detected by XRD, which possibly indicates that the supported Pd NPs had ultrasmall particle sizes and were highly dispersed on the support.

Raman spectroscopy is a fast and nondestructive characterization technique to characterize the structure and quality of carbon materials [33]. Fig. 1(b) showed the Raman spectra of pre-NCF, pre-NC, NCF, NC, Pd/NCF and Pd/NC, exhibiting a G band at *ca.* 1590 cm^{-1} and a D band at *ca.* 1350 cm^{-1} [34]. It is known that the G band resulting from the E_{2g} vibration mode of sp^2 carbon domains is indicative of the extent of its graphitization, whereas the D band is related to structural imperfections and partially disordered states of the sp^2 domains [35,36]. The ratio of D and G band intensities (I_D/I_G) can be used to evaluate the degree of graphitization of carbon-based materials [37]. The Raman spectra of pre-NCF and pre-NC shows that the prepolymers obtained after hydrothermal treatment had been carbonized to some extent. The I_D/I_G of the prepolymer pre-NCF was 1.02 and the I_D/I_G of the product NCF after carbonization was 1.04, which was merely 2% increase. In contrast, the I_D/I_G of NC increased by 3.8% after carbonation (from 1.06 to 1.10). This indicates that the structural integrity of chitosan can be maintained after the addition of F127. Moreover, Pd/NCF exhibited smaller I_D/I_G values than Pd/NC, implying the addition of F127 is capable of promoting the graphitization of the carbon material, which correspond to the XRD results.

FTIR spectra (Fig. 1(c)) indicates that the broad absorption peak of CTS at 3409.5 cm^{-1} was mainly attributable to the ν(O—H) stretching vibration and some ν(N—H) stretching vibration, indicative of intra- or intermolecular hydrogen bonds [38]. However, the broad characteristic peak of pre-NC was blue-shifted compared with CTS, suggesting that the intra- or intermolecular hydrogen bonding of CTS (induced by —OH and —NH_2) was weakened after hydrothermal prepolymerization. In contrast, the red-shift of the absorption peak of pre-NCF was attributed to the fact that —OH and —NH_2 on the CTS molecular segments combined with the terminal —OH on F127 or oxygen on polyethylene oxide in a manner that formed hydrogen bonds. In addition, the vibration peak of the free amino group at 1670.0 cm^{-1} in pre-NCF was substantially enhanced compared with that in pre-NC; indicating that F127 can increase the amino group content in pre-NCF, which provides an opportunity to increase the N content in nitrogen-doped carbon. In addition, the spectra of NCF and NC show great similarity, demonstrating the decomposition of F127 after carbonization. That is, the presence of F127 enhances the hydrogen bonding between CTS and F127 and fixes the N in the free amino group.

The specific surface area and pore structure of the supports and catalysts were calculated by N_2 adsorption–desorption isotherms. NC and NCF exhibited type I and type IV isotherms, respectively (Fig. 1(d)), indicating that NC exhibited microporous properties, and that NCF exhibited microporous as well as mesoporous properties [39]. The specific surface area of NC and NCF were calculated as 330 and 211 $m^2 \cdot g^{-1}$, respectively. These differences may be due to the variation of pore structure. Pore size distribution diagram also indicated that F127 can promote the formation of carbon materials with mesoporous structures. The mesoporous pores in the catalyst provide a channel for the rapid transfer of substrate/product [40,41]. In addition, the surface area of Pd/NCF and Pd/NC (Table S1 in Supplementary Material) was slightly less than those of NCF and NC, indicating that the Pd NPs were successfully loaded on the supports.

The size and shape of Pd NPs on the Pd/NCF and Pd/NC catalysts were identified by TEM (Fig. 2(a)–(d)). Statistical analysis revealed that the ultrasmall Pd NPs were uniformly dispersed on NCF and NC with an average diameter of 4.5 and 3.8 nm, respectively. There

Table 1
Comparison of recently reported Pd-based catalysts towards the OCP reaction

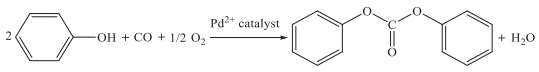

Catalysts	Phenol conversion/%	DPC selectivity/%	DPC yield/%	Ref.
Pd/NCF	45.9	87.9	40.3	This work[①]
Re-Pd/NCF	43.2	85.3	36.8	
Pd/NC	60.4	84.5	51.0	This work[①]
Re-Pd/NC	29.6	63.9	18.9	
Pd/CeO_2-T	53.2	96.7	51.4	[6]
Re-Pd/CeO_2-T	35.6	42.4	15.1	
Pd-O/CeO_2-NT	67.7	93.3	63.2	[10]
Re-Pd-O/CeO_2-NT	29.3	62.3	18.3	
Pd-Ce-O/SiO_2	64.4	83.4	53.7	[11]
Re-Pd-Ce-O/SiO_2	24.0	23.3	5.6	
PS-MnCe	34.5	99.2	34.2	[29]
Re-PS-MnCe	26.7	98.3	26.2	
Pd/20%MnAMPV_5/MK	24.7	99.1	24.5	[30]
Re-Pd/20%MnAMPV_5/MK	15.9	98.0	15.6	

[①] Reaction conditions: 0.5 g catalyst (Pd 0.047 mmol), phenol 25.5 mmol, CH_2Cl_2 20 ml, 4A molecular sieve 4.0 g, TBAB/H_2BQ/Cu$(OAc)_2$/Pd = 45/45/5/1 in molar ratio, 100 °C, 6 h, CO 6.6 MPa, O_2 0.6 MPa.

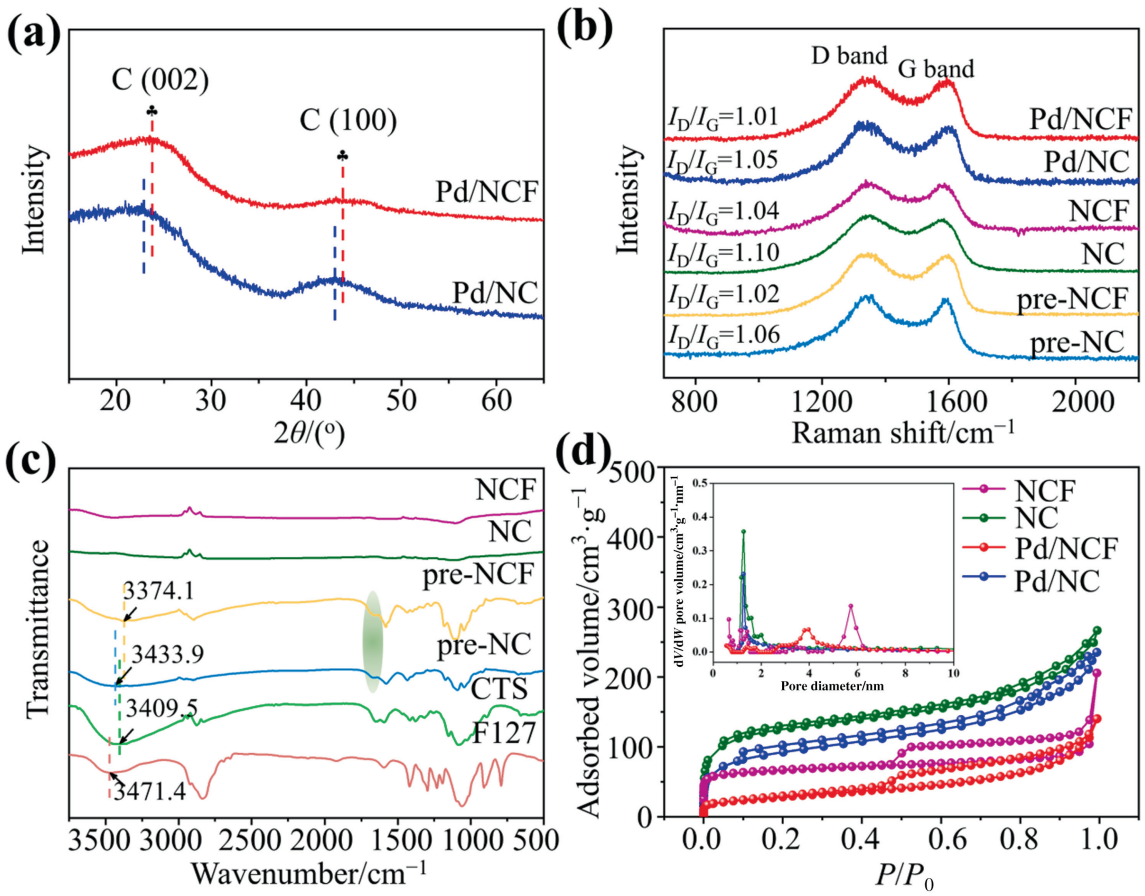

Fig. 1. (a) XRD patterns of Pd/NCF and Pd/NC fresh catalysts. (b) Raman spectra of pre-NCF, pre-NC, NCF, NC, Pd/NCF and Pd/NC. (c) FTIR spectra of CTS, F127, pre-NCF, pre-NC, NCF and NC. (d) Nitrogen sorption isotherms of NCF, NC, Pd/NCF and Pd/NC samples and insets were pore size distribution.

was no substantial change in the particle size of the Pd NPs after using F127 as a stabilizer. HAADF-STEM (Fig. 2(b)) indicates that the NCF support consists mainly of C and N elements. The catalytic activity center, Pd NPs, were well-dispersed on NCF. The quantity of loading of Pd in Pd/NCF and Pd/NC measured by ICP–OES was 0.92% and 0.84%, respectively, indicating that the Pd/NCF prepared with F127 as a stabilizer can anchor more palladium compared with Pd/NC (Table 2). Furthermore, the metal dispersions of Pd/NCF and Pd/NC were characterized by CO pulse adsorption analysis. As shown in Table 2, the metal dispersion of Pd/NCF was 43.8%, which was slightly smaller than that of Pd/NC (45.3%), which may lead to a slightly lower catalytic activity of Pd/NCF than that of Pd/NC.

The chemical compositions and valence states of Pd/NCF and Pd/NC were studied by XPS. Full-range XPS spectra (Fig. S1) demonstrate the existence of Pd, C, O, and N elements on the Pd/NCF and Pd/NC surface; the faint Cl 2p peak was derived from a few unwashed precursors. The high-resolution C 1s spectra were fitted to three peaks at 284.8, 285.8, and 289.0 eV, which could be assigned to C═C, C—N/C═N, and O—C═O, respectively (Fig. S2). The main peak at 284.8 eV originates sp^2-hybridized graphitic carbon atoms [42]. The peaks at 285.8 eV and 289.0 eV are attributed to C atoms bound to N and O atoms, respectively [43]. This may have resulted from the partial decomposition of the polysaccharide structure of the biopolymer. These results confirm that the carbon structures of the Pd/NCF and Pd/NC catalysts are very similar and both have a certain degree of graphitization.

The N 1s spectra exhibited four fitted peaks at 398.4, 400.0, 401.1, and 402.8 eV in Fig. 3(a); assigned to pyridinic N (N-6), pyrrolic N (N-5), graphitic N (N-Q), and oxidized N (N-O), respectively [27,44]. Usually, in N-6 structure the N atom is sp^2 hybridized with two C atoms whereas N-5 is sp^3 hybridized in a five-member ring [45]. In the N-Q structure, an N atom is substituted for a C atom in the graphite structure [46]. The content of various nitrogen species was analyzed by XPS (Fig. 3(b) and Table S2). The content of N-6 in Pd/NCF was larger than that in Pd/NC. N-6 acts as an anchor and a dispersant in a manner that facilitates loading of more Pd for the carrier, also confirmed by the ICP results. The N content of the catalysts was determined by XPS and elemental analysis (Table 2). The surface N content of Pd/NCF obtained by XPS was 4.48%, which is less than the bulk N content measured by elemental analysis (5.99%), indicating that N species were more enriched in the skeleton structure than on the surface. Additionally, the higher N content in Pd/NCF than Pd/NC was attributed to the fact that the reaction between F127 and the amino group of chitosan prevented loss of N, which is compatible with the FTIR spectra results. The abundance of N species in NCF provides the basis for anchoring Pd NPs.

In the Pd 3d spectra of Pd/NCF and Pd/NC (Fig. 3(c)), 335.9 and 341.2 eV are attributed to Pd^0, and 337.7 and 342.9 eV are attributed to Pd^{2+}, indicating that Pd^0 and Pd^{2+} species coexist [47]. Compared with known values for PdO compounds (*ca.* 337.2 and 342.4 eV) [48], a positive shift of the Pd^{2+} peaks was observed in the Pd 3d spectra of the Pd/NCF and Pd/NC. The reason for this difference could be the presence of additional chlorine ligands (chlorine was detected by XPS survey spectra). Furthermore, the percentage of Pd^{2+} on the surface of Pd/NCF (42.0%) was less than that of Pd/NC (78.7%), which could be because of the comparatively

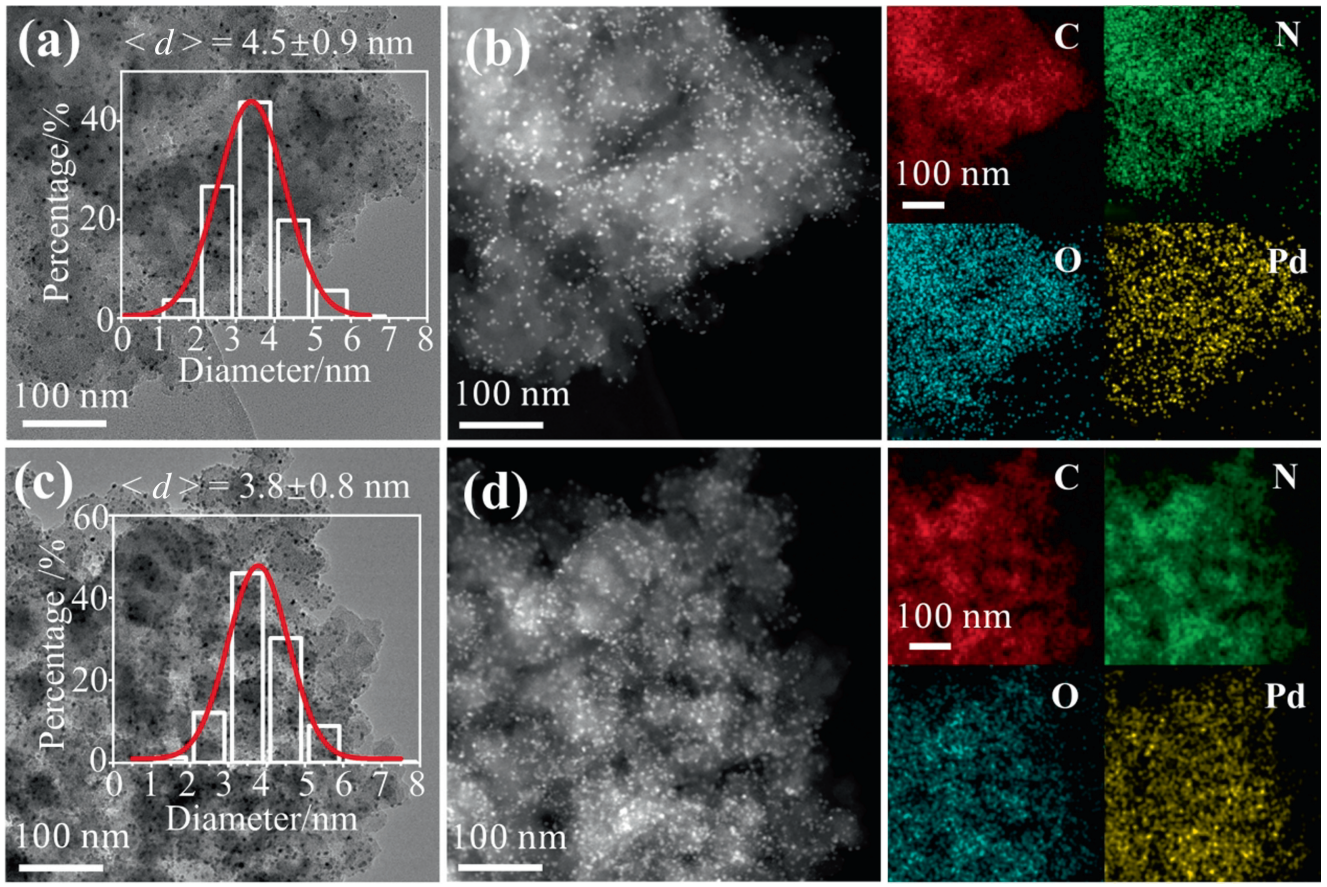

Fig. 2. TEM images of (a) Pd/NCF and (c) Pd/NC fresh catalysts. HAADF–STEM images and corresponding elemental mappings images of (b) Pd/NCF and (d) Pd/NC fresh catalysts. Insets: size distributions of Pd nanoparticles.

Table 2
Structural parameters of the catalysts

Catalysts	N species/%		Pd species/%				Pd particle size/nm		Metal dispersion⑤/%
	N①	N②	Pd③	Pd②	Pd^{2+}④	Pd^{0}④	XRD	TEM	
Pd/NCF	5.99	4.48	0.92	0.86	42.0	58.0	–	4.5	43.8
Pd/NC	4.78	3.08	0.84	0.73	78.7	21.3	–	3.8	45.3
Re-Pd/NCF	4.65	2.81	0.80	0.76	33.2	66.8	6.1	5.3	38.1
Re-Pd/NC	2.78	1.42	0.35	0.30	42.0	58.0	13.5	8.0	25.2

① Determined from element analysis.
② Determined from XPS analysis.
③ Determined from ICP-OES.
④ Relative content of Pd calculated from Pd 3d XPS spectra.
⑤ Determined by CO pulse adsorption analysis.

high nitrogen content of the former. Nitrogen atoms exhibit electron-donor properties and could transfer some of their electron density to Pd, thereby increasing the percentage of Pd^0 [49]. Because of the fact that the active center of DPC synthesized by OCP is Pd^{2+}, the catalytic activity of Pd/NC is superior. Thus, the nitrogen-doped carbon prepared by adding F127 affected the Pd valence distribution and thus the activity. In addition, the slightly lower Pd 3d binding energy of Pd/NCF compared to Pd/NC can be explained by the stronger interaction between Pd NPs and NCF support owing to the Pd–N coordination [50]. The high affinity of Pd toward forming σ or π bonds with N-containing ligands has been reported in Ref. [51]. The strong interactions between Pd and N can facilitate dispersion and stability of the metal active components, and electronic structures are modified.

3.2. Stability of catalysts

The reusability of the Pd/NCF and Pd/NC catalysts were then evaluated. After four cycles, Pd/NCF maintained 71.3% of the initial yield, while Pd/NC only held its initial yield of 4.5%, indicating that the catalytic stability of Pd/NCF was better than that of Pd/NC (Fig. S3). Notably, the recently reported Pd-based catalysts for OCP often deactivate rapidly after only one reaction. In our work, after two cycles, the yield of Pd/NCF was 91.3% of the initial yield, which is more stable than most of the reported catalysts (Table 1). In contrast, the Pd/NC catalyst loses about two-thirds of the DPC yield after two cycles. Considering that the Pd/NC catalyst showed a rapid decrease in activity after two cycles and almost no catalytic activity after four cycles, a series of characterizations of catalysts

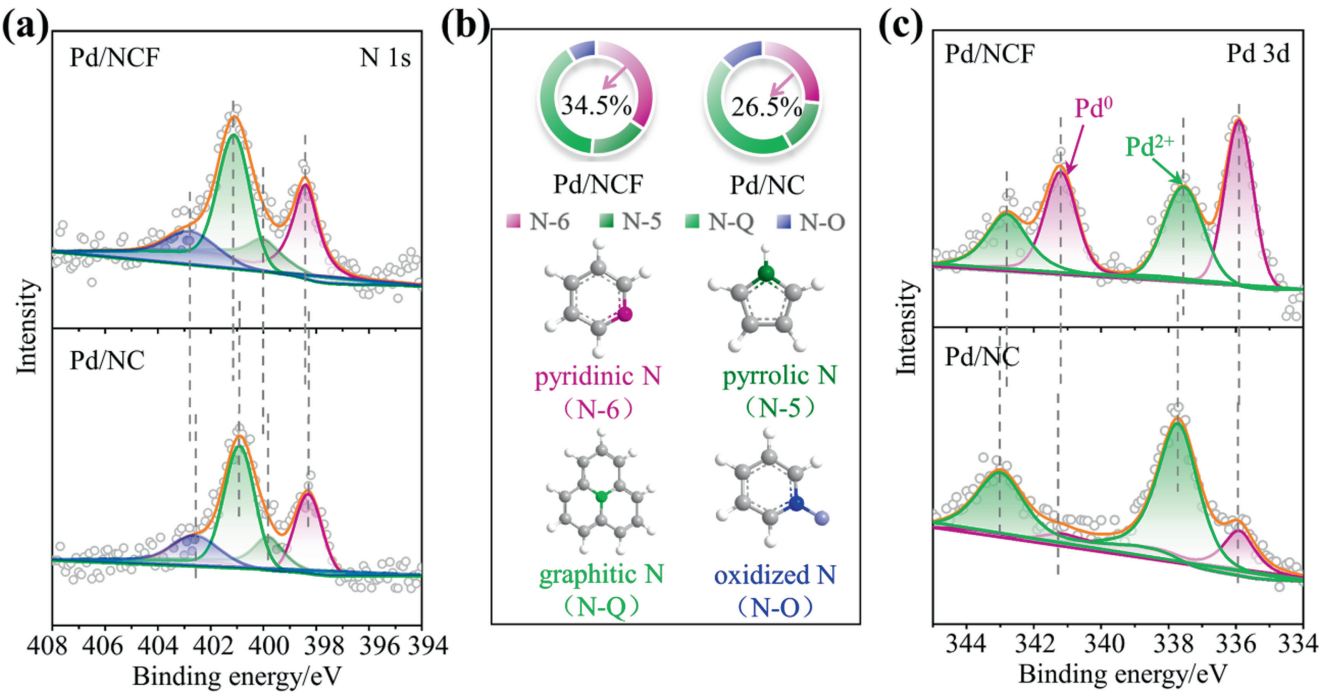

Fig. 3. (a) XPS N 1s spectra and (b) corresponding-N content percentages of Pd/NCF and Pd/NC catalysts. (c) Pd 3d spectra of Pd/NCF and Pd/NC catalysts.

after the second cycle were performed to clarify the reason for the enhanced stability after adding F127. The recovered catalysts after the second cycle were denoted as Re-Pd/NCF and Re-Pd/NC, respectively.

As aforementioned, the XRD and Raman spectra of fresh catalysts Pd/NCF and Pd/NC indicate that adding F127 increased the graphitization degree of the carbon materials. The increase in the graphitization degree of carbon materials increases the number of π sites (which can act as anchoring centers for metal NPs), and enhances resistance to sintering of Pd NPs in supports [52,53]. Therefore, compared with Pd/NC, the metal–support interaction in the Pd/NCF catalyst was improved, and the stability of the catalyst was substantially enhanced.

The recovered catalysts Re-Pd/NCF and Re-Pd/NC were characterized to clarify the reason for the enhanced stability after adding F127. Fig. S4 shows that the carbon peaks of the two recovered catalysts are not significantly different in the XRD patterns. Notably, the diffraction peaks were observed at 40.0°, 46.5°, and 67.9°, corresponding to the characteristics of Pd NPs for (1 1 0), (2 0 0), and (2 2 0) lattice planes of Pd crystal (PDF#88-2335) with face centered cubic (fcc) structures, respectively [14]. According to the Scherrer's formula $D = k\lambda/\beta\cos\theta$ and half-width of Pd (1 1 1) peak, the calculated average sizes of Pd nanoparticles in Re-Pd/NCF and was 6.1 nm (Table 2), respectively, obviously smaller than 13.5 nm of Re-Pd/NC. This indicates that the partial Pd^{2+} is converted to Pd^0 and the Pd NPs increase due to an excess of the reducing gas, CO, filling the reaction system for Pd/NCF and Pd/NC catalysts after the reaction. However, the Pd nanoparticles of Pd/NCF did not substantially increase in size after the reaction, whereas Pd/NC did (Table 2).

The valence states of N as well as Pd content in the Re-Pd/NCF and Re-Pd/NC recovered catalysts were determined by the XPS. Fig. S5 showed the presence of Pd, C, N, and O elements in all samples. Moreover, the N 1s spectra indicate that the surface N content of Re-Pd/NCF was higher than that of Re-Pd/NC (Fig. 4(a) and Table 2). The content of N-6 (which acts as an anchor and dispersant for the Pd NPs) in Re-Pd/NCF (28.1%) exceeded that of Re-Pd/NC (21.5%), see Fig. 4(b). The most direct result is that the Pd content of Re-Pd/NCF (0.76%) was substantially higher than that of Re-Pd/NC (0.30%) (Fig. 4(c) and Table 2). This is a main reason why the Pd/NCF catalyst was stable and exhibited excellent reusability. The Pd^{2+} ratio of Pd/NCF decreased from 44.0% (pre-reaction) to 33.2% (post-reaction), a 10.8% decrease. The Pd^{2+} ratio of Pd/NC decreased from 78.7% (pre-reaction) to 42.0% (post-reaction), a 36.7% decrease. The larger decrease in the Pd content and the relative proportion of Pd^{2+} were the principal reasons for the deactivation of the Pd/NC catalyst. That is, pyridine N plays a crucial role in stabilizing Pd^{2+} species. Wang *et al.* [18] reported that the stability of cationic Pd on a support was improved by constructing Pd–N ligands with pyridinic N. Hu *et al.* [54] also pointed out thatN-doping stabilizes the oxidized Ru specie.

Fig. 5(a) and (c) shows TEM images of Re-Pd/NCF and Re-Pd/NC, respectively. The TEM image for Re-Pd/NC (Fig. 5(d)) indicates larger sizes and broader size distributions of (8.0 ± 4.3) nm compared with Pd/NC ((3.8 ± 0.8) nm). However, the dispersion and particle size distribution of the Pd NPs in Re-Pd/NCF were not much different from those in Pd/NCF; the Pd NPs remained homogeneously dispersed with a small particle size and narrow size distribution ((5.3 ± 1.3) nm) on the NCF surface in Re-Pd/NCF, further confirmed by HAADF–STEM image (Fig. 5(b)). This is related to the NCF support provided a sufficient number of N sites for deposition of active-center Pd NPs after recovery. This interpretation can be demonstrated by the previous analysis of the N content. Thus, the N sites played an important role in stabilizing Pd NPs on the support, which improved the metal dispersion. In addition, the metal dispersion of 38.1% for Re-Pd/NCF is much better than that of 25.2% for Re-Pd/NC (Table 2), in excellent agreement with the TEM results. The small size and uniform distribution of the Pd NPs enabled sufficient interactions between the catalytic sites and facilitated the high performance of the catalyst [55].

Based on ICP analysis, the Pd content of the recovered Re-Pd/NCF catalyst retained 87% of the Pd content relative to that of the fresh Pd/NCF catalyst (Table 2). This result can be attributed to a sufficient quantity of N to firmly anchor the Pd NPs on the

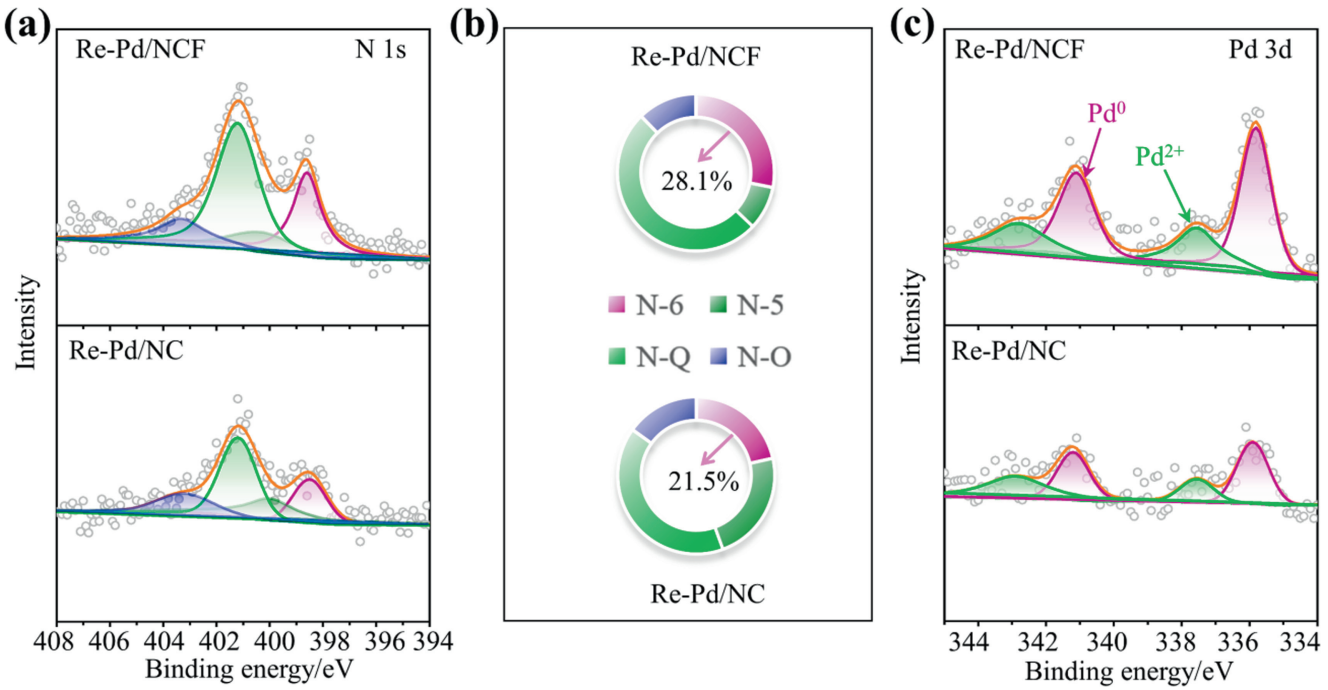

Fig. 4. (a) XPS N 1s spectra and (b) corresponding N-content percentages of Re-Pd/NCF and Re-Pd/NC recovered catalysts. (c) Pd 3d spectra of Re-Pd/NCF and Re-Pd/NC.

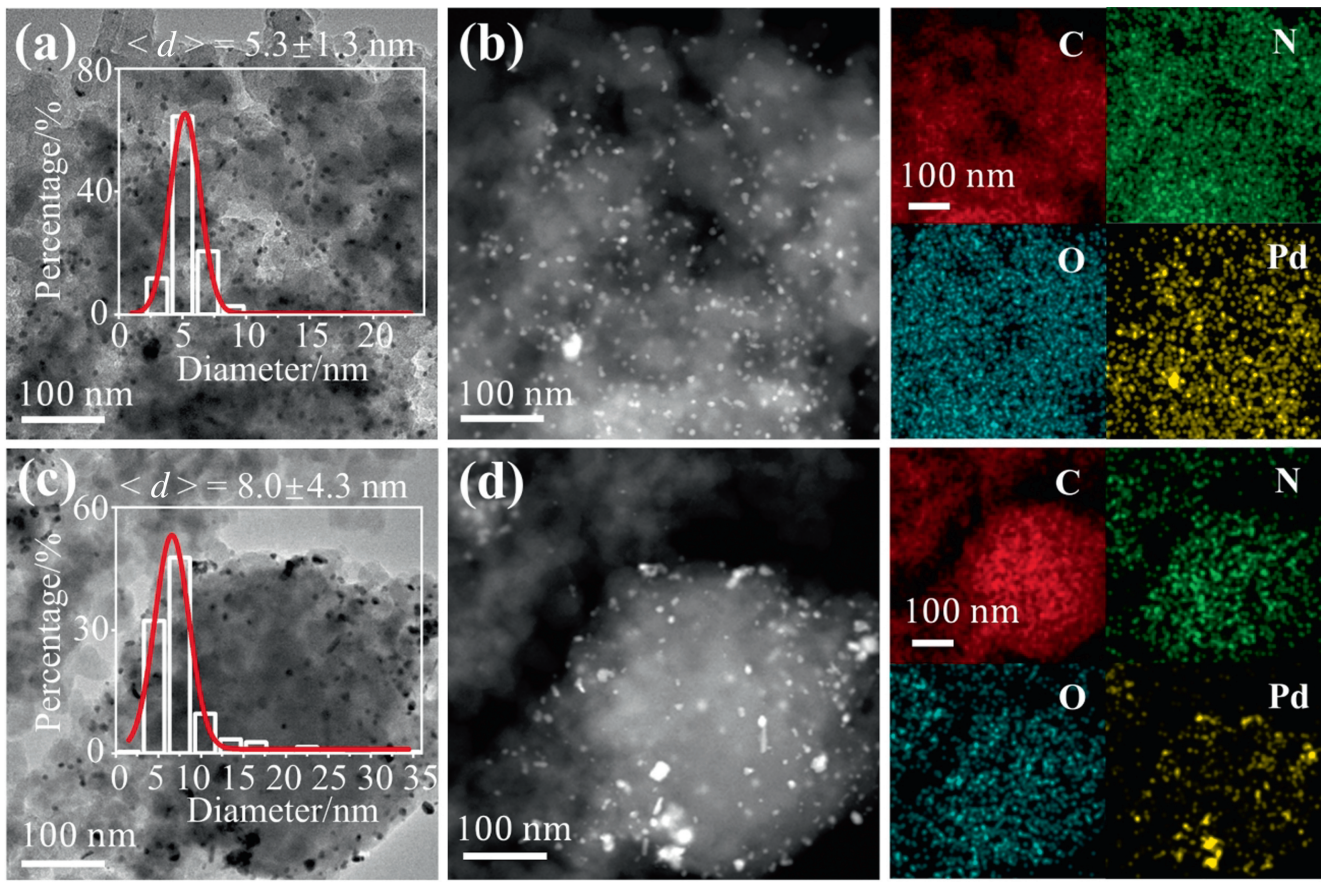

Fig. 5. TEM images of (a) Re-Pd/NCF and (c) Re-Pd/NC. HAADF-STEM images and the corresponding elemental mappings images of (b) Re-Pd/NCF and (d) Re-Pd/NC. Insets: size distributions of Pd nanoparticles.

nitrogen-doped carbon-support as well as to enhance the interactions between Pd and the support; thus, leaching of Pd NPs in the catalyst was prevented and the stability was drastically enhanced. In contrast, the Pd content of Re-Pd/NC was less than half that of Pd/NC, and the content of Pd^{2+} (the active center) was dramatically reduced; both of which are responsible for the significant decreased activity of Pd/NC.

The results reveal that N acted as an anchoring point for the Pd NPs on the support, and in particular, pyridine N was essential for stabilizing Pd^{2+}. Therefore, the type of N that is responsible for stabilizing Pd^{2+} on the carbon support, thereby enhancing the stability of the catalyst, is an important question. In general, a Pd atom readily interacts with two pyridine N atoms; thus, two pyridine N atoms were included in the N-6 model [44]. Fig. 6 shows adsorption models of Pd^{2+} on a carbon support of four types of nitrogen: *i.e.*, N-6, N-5, N-Q, and N-O. The adsorption energy (E_{ads}) of Pd^{2+} on N-6 (−5.50 eV) was higher than that of N-5 (−4.89 eV) and N-O (−1.93 eV), indicating that the presence of pyridine N substantially stabilized the Pd^{2+} species on the carbon support. In addition, the Pd atom located above the graphitic N site in the initial configuration moved to the adjacent carbon sites and formed a bridge above the C—C bond, indicating that N-Q is not a suitable site for anchoring Pd NPs.

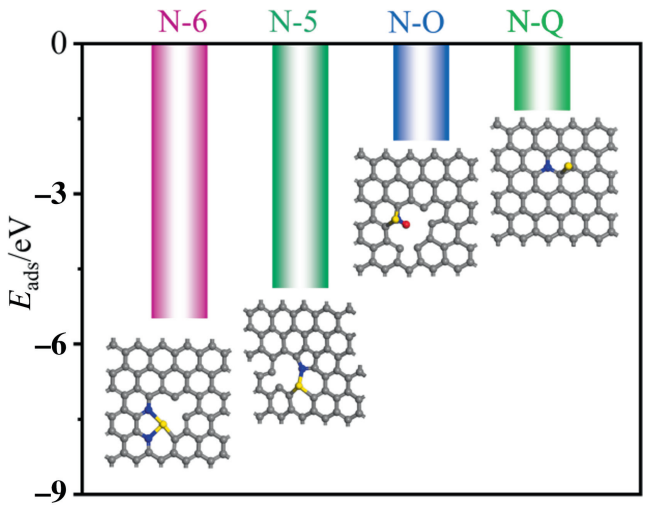

Fig. 6. Optimized structure for Pd^{2+} on (a) pyrrolic (N-5), (b) pyridinic (N-6), (c) oxidized N (N-O), and (d) graphitic N (N-Q) of the carbon support. Gray, blue, red, and yellow spheres represent C, N, O, and Pd atoms, respectively.

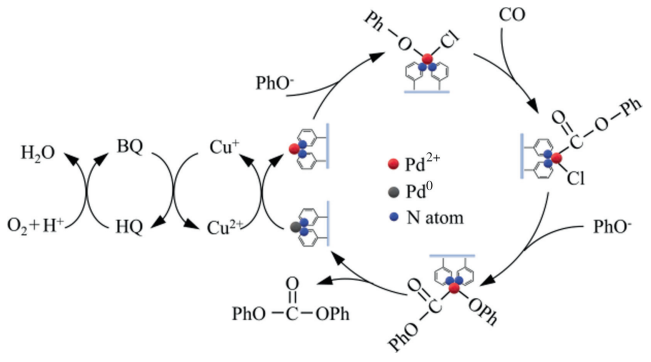

Fig. 7. Mechanism of oxidative carbonylation of phenol catalyzed by Pd/NCF.

3.3. Possible reaction mechanism of Pd/NCF

The reaction mechanism of OCP to DPC over Pd/NCF catalyst can be inferred based on the aforementioned catalyst characterization results and previous reports [8,10]. Based on the reported reaction mechanism of the OCP reaction, the role of Pd/NCF catalyst in this reaction was studied, as shown in Fig. 7.

The OCP reaction is a multi-step electron transfer reaction. At first, Pd^{2+} is first anchored by pyridine N atoms and then reacts with PhO^- to form PhO—Pd—Cl, followed by the insertion of CO into the Pd—O bond to form the intermediate PhOCOPdCl, and another PhO^- replaces Cl^- to form PhOCOPdOPh, and finally the product DPC is obtained after the reduction-elimination reaction. At the same time, active center, Pd^{2+}, is converted to Pd^0 and lost its catalytic activity. Then Pd^0 is converted into Pd^{2+} by multi-stage oxidation of Cu^+/Cu^{2+} and benzoquinone (BQ)/hydroquinone (HQ) and achieves the cyclic conversion of Pd^{2+} and Pd^0, so that the phenol oxidation carbonylation reaction continues. Leaching, reduction and agglomeration of Pd species are the main causes of catalyst deactivation, therefore our main aim was to stabilize Pd^{2+} and ensure uniform dispersion of Pd NPs on the support during the reaction. Elemental analysis and XPS results showed that the addition of F127 increased the N content of the carbon material, ensuring that the support could provide sufficient N sites for the deposition of the active center Pd NPs. Based on ICP analysis, the loss of Pd species is significantly inhibited in Pd/NCF during the reaction process. In addition, the high N content and the high degree of graphitization and mesoporous structure in Pd/NCF catalyst help to maintain the small size and uniform dispersion of Pd NPs, as demonstrated by TEM results and CO pulse chemisorption. After the reaction, Pd^0 was more easily oxidized to Pd^{2+} by the co-catalyst. Pyridine N in Pd/NCF catalyst stabilized the Pd^{2+} species and thus improved the stability of the Pd/NCF catalyst. In contrast, the reduced N content in the Re-Pd/NC catalyst led to increased size and aggregation of Pd NPs, so that only the surface Pd^0 is re-oxidized while the internal Pd^0 remains, resulting in the deactivation of the Pd/NC catalyst.

4. Conclusions

NCF was prepared by using chitosan as the carbon and nitrogen source, and F127 as the stabilizer; and was used as the support to prepare a Pd nanoparticle (Pd/NCF) catalyst for OCP. The stability of the Pd/NCF catalyst was much higher than that of most reported Pd-based catalysts. There was only an 8.7% decrease of the DPC yield after recovery of the catalyst. Adding F127 increased the N content of the carbon material, ensuring firm anchoring of the Pd nanoparticles on the support, which improved the Pd NP dispersion and leaching. Moreover, introducing F127 increased the graphitization of the carbon material, which drastically decreased the sintering rate of the metal nanoparticles and enhanced the metal-support interactions. Furthermore, the interactions of Pd^{2+} species with the pyridine N atom prevented oxidation of active-center Pd^{2+} and improved the stability. This work provides insight into enhancing the stability of supported metal catalysts.

Data Availability

Data will be made available on request.

Declaration of Competing Interest

The authors declare that they have no known competing financial interests or personal relationships that could have appeared to influence the work reported in this paper.

Acknowledgements

Thanks for the support by the National Natural Science Foundation of China (U21A20306, U20A20152), and Natural Science Foundation of Hebei Province (B2022202077). We thank Michael Scott Long, PhD, from Liwen Bianji (Edanz) (www.liwenbianji.cn) for editing the English text of a draft of this manuscript.

Supplementary Material

Supplementary material to this article can be found online at https://doi.org/10.1016/j.cjche.2023.08.001.

References

[1] M.Q. Gao, Z.R. Yang, H.J. Zhang, J.H. Ma, Y.D. Zou, X.W. Cheng, L.M. Wu, D.Y. Zhao, Y.H. Deng, Ordered mesopore confined Pt nanoclusters enable unusual self-enhancing catalysis, *ACS Cent. Sci.* 8 (12) (2022) 1633–1645.
[2] L.M. Cao, J. Zhang, X.F. Zhang, C.T. He, Confinement synthesis in porous molecule-based materials: A new opportunity for ultrafine nanostructures, *Chem. Sci.* 13 (6) (2022) 1569–1593.
[3] X. Sun, F. Li, Z.M. Wang, H.L. An, W. Xue, X.Q. Zhao, Y.J. Wang, Fast hydrogen evolution by formic acid decomposition over AuPd/TiO_2-NC with enhanced stability, *Int. J. Hydrog. Energy* 48 (35) (2023) 13000–13011.
[4] B. Hu, L. Warczinski, X.Y. Li, M.H. Lu, J. Bitzer, M. Heidelmann, T. Eckhard, Q. Fu, J. Schulwitz, M. Merko, M.S. Li, W. Kleist, C. Hättig, M. Muhler, B.X. Peng, Formic acid-assisted selective hydrogenolysis of 5-hydroxymethylfurfural to 2,5-dimethylfuran over bifunctional Pd nanoparticles supported on N-doped mesoporous carbon, *Angew. Chem. Int. Ed.* 60 (12) (2021) 6807–6815.
[5] B. Hu, L. Warczinski, X. Li, M. Lu, J. Bitzer, M. Heidelmann, T. Eckhard, Q. Fu, J. Schulwitz, M. Merko, M. Li, W. Kleist, C. Hattig, M. Muhler, B. Peng, Formic acid-assisted selective hydrogenolysis of 5-hydroxymethylfurfural to 2,5-dimethylfuran over bifunctional Pd nanoparticles supported on N-doped mesoporous carbon, *Angew. Chem. Int. Ed.* 60 (12) (2021) 6807–6815.
[6] Z.J. Fu, Z.M. Wang, H.J. Wang, F. Li, W. Xue, Y.J. Wang, Pd catalyst supported on CeO_2 nanotubes with enhanced structural stability toward oxidative carbonylation of phenol, *RSC Adv.* 9 (20) (2019) 11356–11364.
[7] X.J. Yang, Y. Hu, H. Bai, M.Q. Feng, Z.G. Yan, S. Cao, B. Yang, Tuning of oxygen species and active Pd^{2+} species of supported catalysts *via* morphology and Mn doping in oxidative carbonylation of phenol, *Mol. Catal.* 457 (2018) 1–7.
[8] L.C. Zhou, G. Feng, X.J. Liu, Z.M. Wang, F. Li, W. Xue, Y.J. Wang, Effect of Zr-doping on Pd/$Ce_xZr_{1-x}O_2$ catalysts for oxidative carbonylation of phenol, *Chin. J. Chem. Eng.* 28 (10) (2020) 2592–2599.
[9] C.F. Yin, J. Zhou, Q.M. Chen, J.Y. Han, Y.X. Wu, X.J. Yang, Deactivation causes of supported palladium catalysts for the oxidative carbonylation of phenol, *J. Mol. Catal. A* 424 (2016) 377–383.
[10] Y. Yuan, Z.M. Wang, H.L. An, W. Xue, Y.J. Wang, Oxidative carbonylation of phenol with a Pd-O/CeO_2-nanotube catalyst, *Chin. J. Catal.* 36 (7) (2015) 1142–1154.
[11] Z.M. Wang, H.Q. Zhang, L.C. Zhou, F. Li, W. Xue, Y.J. Wang, Role of Ce in supported Pd catalyst for oxidative carbonylation of phenol to diphenyl carbonate, *CIESC J.* 70 (12) (2019) 4625–4634. (in Chinese)
[12] Y. Rangraz, M.M. Heravi, A. Elhampour, Recent advances on heteroatom-doped porous carbon/metal materials: Fascinating heterogeneous catalysts for organic transformations, *Chem. Rec.* 21 (8) (2021) 1985–2073.
[13] K. Yan, D. Wang, H. Li, Atom doping engineering of metal/carbon catalysts for biomass hydrodeoxygenation, *ACS Sustain. Chem. Eng.* 9 (2021) 16531–16555.
[14] X.X. Li, Q.S. Zhao, X. Feng, L. Pan, Z.Z. Wu, X.C. Wu, T.W. Ma, J.L. Liu, Y.Y. Pan, Y. Song, M.B. Wu, Pyridinic nitrogen-doped graphene nanoshells boost the catalytic efficiency of palladium nanoparticles for the N-allylation reaction, *ChemSusChem* 12 (4) (2019) 858–865.
[15] H.Y. Song, E.D. Park, J.S. Lee, Oxidative carbonylation of phenol to diphenyl carbonate over supported palladium catalysts, *J. Mol. Catal. A* 154 (1–2) (2000) 243–250.
[16] C.P. Wang, Z. Wang, S.J. Mao, Z.R. Chen, Y. Wang, Coordination environment of active sites and their effect on catalytic performance of heterogeneous catalysts, *Chin. J. Catal.* 43 (4) (2022) 928–955.
[17] Z.L. Jiang, S.J. Song, X.B. Zheng, X. Liang, Z.X. Li, H.F. Gu, Z. Li, Y. Wang, S.H. Liu, W.X. Chen, D.S. Wang, Y.D. Li, Lattice strain and Schottky junction dual regulation boosts ultrafine ruthenium nanoparticles anchored on a N-modified carbon catalyst for H_2 production, *J. Am. Chem. Soc.* 144 (42) (2022) 19619–19626.
[18] B.L. Wang, Y.X. Yue, C.X. Jin, J.Y. Lu, S.S. Wang, L. Yu, L.L. Guo, R.R. Li, Z.T. Hu, Z. Y. Pan, J. Zhao, X.N. Li, Hydrochlorination of acetylene on single-atom Pd/N-doped carbon catalysts: Importance of pyridinic-N synergism, *Appl. Catal. B* 272 (2020) 118944.
[19] X. Kan, X.P. Chen, W. Chen, J.X. Mi, J.Y. Zhang, F.J. Liu, A.M. Zheng, K.A. Huang, L. J. Shen, C. Au, L.L. Jiang, Nitrogen-decorated, ordered mesoporous carbon spheres as high-efficient catalysts for selective capture and oxidation of H_2S, *ACS Sustain. Chem. Eng.* 7 (8) (2019) 7609–7618.
[20] X. Kan, F.Y. Song, G.Q. Zhang, Y. Zheng, Q.L. Zhu, F.J. Liu, L.L. Jiang, Sustainable design of co-doped ordered mesoporous carbons as efficient and long-lived catalysts for H_2S reutilization, *Chem. Eng. Sci.* 269 (2023) 118483.
[21] S.J. Mao, C.P. Wang, Y. Wang, The chemical nature of N doping on N doped carbon supported noble metal catalysts, *J. Catal.* 375 (2019) 456–465.
[22] Y. Sheth, S. Dharaskar, M. Khalid, S. Sonawane, An environment friendly approach for heavy metal removal from industrial wastewater using chitosan based biosorbent: A review, *Sustain. Energy Technol. Assess.* 43 (2021) 100951.
[23] J.H. Advani, K. Ravi, D.R. Naikwadi, H.C. Bajaj, M.B. Gawande, A.V. Biradar, Bio-waste chitosan-derived N-doped CNT-supported Ni nanoparticles for selective hydrogenation of nitroarenes, *Dalton Trans.* 49 (30) (2020) 10431–10440.
[24] S.Z. Jia, H.Y. Pan, Q. Lin, X.S. Wang, C.G. Li, M. Wang, Y.Y. Shi, Study on the preparation and mechanism of chitosan-based nano-mesoporous carbons by hydrothermal method, *Nanotechnology* 31 (36) (2020) 365604.
[25] W. Zhang, K.R. Zhu, W.X. Ren, H.L. He, H.C. Liang, Y.P. Zhai, W. Li, Recent advances in the marriage of catalyst nanoparticles and mesoporous supports, *Adv. Mater. Interfaces* 9 (3) (2022) 2101528.
[26] Z.J. Li, T.T. Fan, H.H. Li, X.W. Lu, S.Q. Ji, J.W. Zhang, J.H. Horton, Q. Xu, J.F. Zhu, Atomically defined undercoordinated copper active sites over nitrogen-doped carbon for aerobic oxidation of alcohols, *Small* 18 (11) (2022) e2106614.
[27] L.F. Li, Y.D. Wen, G.K. Han, Y.X. Liu, Y.J. Song, W. Zhang, J. Sun, L. Du, F.P. Kong, Y.L. Ma, Y.Z. Gao, J.J. Wang, C.Y. Du, G.P. Yin, Tailoring the stability of Fe-N-C *via* pyridinic nitrogen for acid oxygen reduction reaction, *Chem. Eng. J.* 437 (2022) 135320.
[28] T. Jin, X.F. Liu, Y.Q. Su, F. Pan, X. Han, H.Y. Zhu, R.Q. Wu, Y. Lyu, Mesoporous carbon-supported ultrasmall metal nanoparticles *via* a mechanochemical-driven redox reaction: A "Two-in-One" strategy, *Appl. Catal. B* 294 (2021) 120232.
[29] M. Peng, C. Hong, N. Cai, Y. Hu, H. Yuan, Effect of metal doping on multi-step electron transfer and oxygen species of silicon-based nanocomposite aerogel supported Pd catalysts in oxidative carbonylation of phenol, *Mol. Catal.* 482 (2020) 110684.
[30] M. Peng, X.J. Yang, J.X. Wu, H.A. Yuan, C.F. Yin, Y.X. Wu, Application of vanadium incorporated phosphomolybdate supported on the modified kaolinin synthesis of diphenyl carbonate by oxidative carbonylation with phenol, *Chem. Ind. Chem. Eng. Q.* 23 (3) (2017) 421–429.
[31] D.T. Chen, L.H. Zhang, J. Du, H.H. Wang, J.Y. Guo, J.Y. Zhan, F. Li, F.S. Yu, A tandem strategy for enhancing electrochemical CO_2 reduction activity of single-atom Cu-S1 N_3 catalysts *via* integration with Cu nanoclusters, *Angew. Chem. Int. Ed. Engl.* 60 (45) (2021) 24022–24027.
[32] Q. Wu, M.M. Gao, G.Y. Zhang, Y.H. Zhang, S.W. Liu, C.X. Xie, H.L. Yu, Y. Liu, L. Huang, S.T. Yu, Preparation and application performance study of biomass-based carbon materials with various morphologies by a hydrothermal/soft template method, *Nanotechnology* 30 (18) (2019) 185702.
[33] Z.H. Sheng, L. Shao, J.J. Chen, W.J. Bao, F.B. Wang, X.H. Xia, Catalyst-free synthesis of nitrogen-doped graphene *via* thermal annealing graphite oxide with melamine and its excellent electrocatalysis, *ACS Nano* 5 (6) (2011) 4350–4358.
[34] P. Pachfule, D. Shinde, M. Majumder, Q. Xu, Fabrication of carbon nanorods and graphene nanoribbons from a metal-organic framework, *Nat. Chem.* 8 (7) (2016) 718–724.
[35] K.N. Kudin, B. Ozbas, H.C. Schniepp, R.K. Prud'homme, I.A. Aksay, R. Car, Raman spectra of graphite oxide and functionalized graphene sheets, *Nano Lett.* 8 (1) (2008) 36–41.
[36] X. Kan, F.Y. Song, F.Y. Li, S.Y. Xiao, F.J. Liu, L.L. Jiang, Solvent-free molten co-assembly of ordered mesoporous carbon for efficiently supported adsorption and separation of SO_2, *J. Mater. Chem. A* 10 (16) (2022) 8817–8825.
[37] K. Zhu, Q. Bin, Y.Q. Shen, J. Huang, D.D. He, W.J. Chen, *In-situ* formed N-doped bamboo-like carbon nanotubes encapsulated with Fe nanoparticles supported by biochar as highly efficient catalyst for activation of persulfate (PS) toward degradation of organic pollutants, *Chem. Eng. J.* 402 (2020) 126090.
[38] A. Zając, J. Hanuza, M. Wandas, L. Dymińska, Determination of N-acetylation degree in chitosan using Raman spectroscopy, *Spectrochim. Acta A Mol. Biomol. Spectrosc.* 134 (2015) 114–120.
[39] M.F. Zeng, S. Yang, Y.L. Chen, M.D. Xu, J. Zhao, T.J. Zhang, K.L. Sun, Z. Yang, P. Zhang, X.Z. Cao, B.Y. Wang, Porous chitosan-derived activated N-doped carbon-supported Pd nanoparticles encaged in Al, Fe pillared montmorillonite as novel heterogeneous catalysts, *Appl. Clay Sci.* 224 (2022) 106520.
[40] W. Guan, Y.L. Zhang, Y. Chen, J.C. Wu, Y. Cao, Y.N. Wei, P.W. Huo, Hierarchical porous bowl-like nitrogen-doped carbon supported bimetallic AuPd nanoparticles as nanoreactors for high efficient catalytic oxidation of HMF to FDCA, *J. Catal.* 396 (2021) 40–53.
[41] F.J. Liu, K. Huang, Q. Wu, S. Dai, Solvent-free self-assembly to the synthesis of nitrogen-doped ordered mesoporous polymers for highly selective capture and conversion of CO_2, *Adv. Mater.* 29 (27) (2017) 1700445.
[42] D. Wang, J. Liu, J.B. Xi, J.Z. Jiang, Z.W. Bai, Pd-Fe dual-metal nanoparticles confined in the interface of carbon nanotubes/N-doped carbon for excellent catalytic performance, *Appl. Surf. Sci.* 489 (2019) 477–484.
[43] Y.Y. Zhu, G.Q. Yu, J. Yang, M. Yuan, D. Xu, Z.P. Dong, Biowaste soybean curd residue-derived Pd/nitrogen-doped porous carbon with excellent catalytic performance for phenol hydrogenation, *J. Colloid Interface Sci.* 533 (2019) 259–267.
[44] D.A. Bulushev, M. Zacharska, E.V. Shlyakhova, A.L. Chuvilin, Y.N. Guo, S. Beloshapkin, A.V. Okotrub, L.G. Bulusheva, Single isolated Pd^{2+} cations supported on N-doped carbon as active sites for hydrogen production from formic acid decomposition, *ACS Catal.* 6 (2) (2016) 681–691.

[45] C. Matei Ghimbeu, V.A. Luchnikov, Hierarchical porous nitrogen-doped carbon beads derived from biosourced chitosan polymer, *Microporous Mesoporous Mater.* 263 (2018) 42–52.
[46] L. He, F. Weniger, H. Neumann, M. Beller, Synthesis, characterization, and application of metal nanoparticles supported on nitrogen-doped carbon: Catalysis beyond electrochemistry, *Angew. Chem. Int. Ed. Engl.* 55 (41) (2016) 12582–12594.
[47] J.X. Zhang, H. Jiang, Y.F. Liu, R.Z. Chen, Tuning surface properties of N-doped carbon with TiO_2 nano-islands for enhanced phenol hydrogenation to cyclohexanone, *Appl. Surf. Sci.* 488 (2019) 555–564.
[48] J.C. Xu, B. Zhang, Y.K. Lu, L.G. Wang, W.Y. Tao, X. Teng, W.S. Ning, Z.K. Zhang, Adsorption desulfurization performance of PdO/SiO_2@graphene oxide hybrid aerogel: Influence of graphene oxide, *J. Hazard. Mater.* 421 (2022) 126680.
[49] X. Xu, H.R. Li, Y. Wang, Selective hydrogenation of phenol to cyclohexanone in water over Pd@N-doped carbon derived from ionic-liquid precursors, *ChemCatChem* 6 (12) (2014) 3328–3332.
[50] L.Y. Zou, Q. Liu, D.Y. Zhu, Y.Q. Huang, Y. Mao, X. Luo, Z.W. Liang, Experimental and theoretical studies of ultrafine Pd-based biochar catalyst for dehydrogenation of formic acid and application of in situ hydrogenation, *ACS Appl. Mater. Interfaces* 14 (15) (2022) 17282–17295.
[51] R. Arrigo, M.E. Schuster, Z.L. Xie, Y. Yi, G. Wowsnick, L.L. Sun, K.E. Hermann, M. Friedrich, P. Kast, M. Hävecker, A. Knop-Gericke, R. Schlögl, Nature of the N-Pd interaction in nitrogen-doped carbon nanotube catalysts, *ACS Catal.* 5 (5) (2015) 2740–2753.
[52] C. Bianchini, P.K. Shen, Palladium-based electrocatalysts for alcohol oxidation in half cells and in direct alcohol fuel cells, *Chem. Rev.* 109 (9) (2009) 4183–4206.
[53] Y. Devrim, E.D. Arıca, Investigation of the effect of graphitized carbon nanotube catalyst support for high temperature PEM fuel cells, *Int. J. Hydrog. Energy* 45 (5) (2020) 3609–3617.
[54] J.Q. Hu, F.M. Wang, Y.W. Li, H.H. Lv, M.S. Sun, Y. Zhai, G.J. Lv, X.B. Zhang, Enhanced catalytic performance of oxidized Ru supported on N-doped mesoporous carbon for acetylene hydrochlorination, *Appl. Catal. A* 623 (2021) 118236.
[55] W. Wu, W. Zhang, Y. Long, J.H. Qin, J.T. Ma, Different transfer hydrogenation pathways of halogenated nitrobenzenes catalyzed by Fe-, Co- or Ni-based species confined in nitrogen doped carbon, *Mol. Catal.* 497 (2020) 111226.